ADVANCED FUNCTIONAL MATERIALS
www.afm-journal.de

Noninvasive Transdermal Vaccination Using Hyaluronan Nanocarriers and Laser Adjuvant

Ki Su Kim, Hyemin Kim, Yunji Park, Won Ho Kong, Seung Woo Lee, Sheldon J. J. Kwok, Sei Kwang Hahn, and Seok Hyun Yun**

Vaccines are commonly administered by injection using needles. Although transdermal microneedles are less invasive promising alternatives, needle-free topical vaccination without involving physical damage to the natural skin barrier is still sought after as it can further reduce needle-induced anxiety and is simple to administer. However, this long-standing goal has been elusive since the intact skin is impermeable to most macromolecules. Here, we show an efficient, noninvasive transdermal vaccination by employing two key innovations: the use of hyaluronan (HA) as vaccine carriers and non-ablative laser adjuvants. Conjugates of a model vaccine ovalbumin (OVA) and HA—HA–OVA conjugates—induced more effective maturation of dendritic cells in vitro, compared to OVA. Following topical administration in the skin, HA–OVA conjugates penetrated into the epidermis and dermis in murine and porcine skins, as revealed by intravital microscopy and fluorescence assay. Topical administration of HA-OVA conjugates significantly elevated both humoral and mucosal antibodies, with peak levels at four weeks. An OVA challenge at week eight elicited strong immune-recall responses. With pre-treatment of the skin using non-ablative fractional laser beams as adjuvant, strong immunization was achieved with much reduced doses of HA–OVA (1 mg kg^{-1} OVA). Our results demonstrate the potential of the noninvasive patch-type transdermal vaccination platform.

1. Introduction

Vaccines provide effective prevention and treatment of many infectious diseases.[1] Presently, the most common method of vaccine administration is by injection using needles and syringes. However, needle-based immunization has several disadvantages. Needle injection is painful, causes needle phobia, leaves dangerous medical waste, and poses the risk of disease transmission by needle reuse. A variety of vaccine delivery systems in various different delivery routes have been investigated to make vaccination safer, simpler, less expensive, and more effective.[2] However, the major challenge in transdermal vaccine delivery comes from intrinsic skin barriers that prevent macromolecules, such as protein-based vaccines, from entering the body. Several methods to break the skin barrier have been suggested, including intradermal needles,[3] powderjet,[4] ultrasound,[5] electrical pulses,[6] and photothermal gold nanoparticles.[7] However, these approaches suffered from invasiveness, low bioavailability, or need for special apparatus. Other nondestructive methods based on transdermal administrations (topical applications), such as cationic liposomes,[8] polymeric nanoparticles,[9] and synthetic protamine[10] have been proposed for high skin penetration, but their standalone effectiveness thus far has been unsatisfactory unless adjuvants, such as immunogenic minerals and emulsions,[11] Toll-like receptor ligands,[12] viral vectors,[9] or toxins,[10,13] are used simultaneously. Unfortunately, many of the currently employed adjuvants cause potentially harmful adverse effects, such as pain and swelling by local inflammation, or fever and immunotoxicity by systemic reaction.[14] Recently, microneedle arrays that contain vaccines and adjuvants in lyophilized forms coated on or embedded in biodegradable polymer matrices have shown enhanced immunization and reduced pain compared to conventional intradermal needles.[15,16] Although promising, microneedles, typically one 600–1000 μm in length, still induce physical disruption of the skin barrier and, therefore, can cause discomfort and require sanitary procedures to prevent infection through the holes in the skin.

The skin is one of the preferred sites for vaccine delivery because of accessibility and the abundance of

Dr. K. S. Kim, S. J. J. Kwok, Prof. S. K. Hahn, Prof. S. H. Yun
Wellman Center for Photomedicine
Massachusetts General Hospital
65 Landsdowne St., UP-5, Cambridge, MA 02139, USA
E-mail: skhanb@postech.edu; syun@hms.harvard.edu
Dr. K. S. Kim, S. J. J. Kwok, Prof. S. K. Hahn, Prof. S. H. Yun
Department of Dermatology
Harvard Medical School
40 Blossom St, Boston, MA 02140, USA
Dr. H. Kim, Dr. W. H. Kong, Prof. S. K. Hahn
Department of Materials Science and Engineering
Pohang University of Science and Technology (POSTECH)
77 Cheongam-Ro, Nam-gu, Pohang, Gyeongbuk 790-784, South Korea
Dr. Y. Park, Prof. S. W. Lee
Division of Integrative Biosciences and Biotechnology
POSTECH
77 Cheongam-Ro, Nam-gu, Pohang, Gyeongbuk 790-784, South Korea
Prof. S. W. Lee
Department of Life Science
POSTECH
77 Cheongam-Ro, Nam-gu, Pohang, Gyeongbuk 790-784, South Korea

DOI: 10.1002/adfm.201504879

antigen-presenting cells (APCs), such as Langerhans cells in the epidermis and dermal dendritic cells (DCs).[17] To boost immune response, several types of adjuvant have been used through inducing damage-associated molecular patterns. Recently, there have been various successful preclinical and clinical trials using laser beams to maximize immune responses, a technique called laser adjuvant.[18–22] There are two regimes: ablative and nonablative. Irradiation with high-energy ablative fractional laser beams boosts the immune response by enhancing the activation and motility of APCs[18] and, also, enables vaccine to be delivered through the perforated skin structure.[19] Nonablative fractional laser adjuvant[21,22] uses much lower energy laser beams focused to the dermis to generate the microthermal activation of APCs, without causing any damage to the stratum corneum and epidermis. While this technique on its own is effectively noninvasive, in practice, additional physically disruptive methods are required to overcome the intact skin barrier, such as microneedle arrays[21] or intradermal injection,[22] to deliver vaccine deep into the skin.

Hyaluronan (HA), a natural macromolecule with intrinsically high permeability into the skin,[23] has been investigated for use as a carrier for transdermal drug delivery. HA is a linear polysaccharide abundant in the extracellular matrix in the skin and is widely used as dermal fillers in dermatologic clinics. HA is one of the most hydrophilic molecules in nature but also has a lipophilic patch domain. The amphiphilic nature enables HA to diffuse through the stratum corneum. HA receptors are highly expressed in skin cells, such as keratinocytes in epidermis and fibroblasts in dermis,[24] which facilitates gradient-enhanced diffusion.[25] The efficient skin penetration of HA has been extensively reported.[23–27] Current understanding is that several factors, such as skin hydration, HA receptor mediated transport, and specific structure of HA, contribute to the transdermal delivery of HA.[23,27] Recently, it is reported that HA can induce the structural change of keratin and the disorder of lipid organization in stratum corneum.[26] While the exact mechanisms remain fully understood, HA has been widely investigated as a delivery agent of small molecular drugs and microsized particles for intranasal delivery of influenza vaccines.[28] Recently, we have shown that HA can serve as a transdermal nanocarrier of macromolecules, such as human growth hormone[27] and nano graphene oxide,[29] as well as chemical drugs and peptides. In the tissue, HA is degraded to small fragments in the skin, releasing the drugs. The fragments are recognized in the body as damage associated molecular pattern (DAMP) molecules,[30,31] which can enhance immune response against antigens.

Here, we demonstrate the capability of HA as an efficient transdermal nanocarrier for noninvasive transdermal vaccination using HA–ovalbumin (OVA) conjugates as a model vaccine. By two-photon microscopy and quantitative fluorescence analysis, we show the efficient penetration of HA–OVA conjugate into murine and porcine skins. We find that HA–OVA conjugates activate naive DCs in vitro much more efficiently than OVA alone and a mixture of HA and OVA. We also find that HA–OVA conjugates induce higher immune response than OVA alone and a mixture of HA and OVA after intramuscular injection, reflecting the adjuvant-like role of HA in the vaccine conjugate. Topical administration of HA–OVA conjugates onto intact murine skins efficiently induces the production of OVA-specific antibodies, in both first and secondary immune responses, which establishes the practical potential of this novel approach for needle-free vaccination. Finally, using laser adjuvant, we can reduce the HA–OVA conjugate dosage required for transdermal vaccination to similar levels used for intramuscular administration, while also eliciting strong mucosal immunity.

2. Results

2.1. Vaccination with OVA Alone Elicits Minimal Immune Response

We first tested transdermal immunization in vivo by OVA alone. Various doses of OVA (20, 200, and 500 μg) were applied to the back skin of mice (BALB/c, $n = 4$ each). After four weeks, the production of humoral (IgG) and mucosal (IgA) OVA-specific antibody in the blood serum was measured to be negligible at all doses up to 500 μg (**Figure 1**a). To boost immunization efficiency, the skin site was illuminated with nonablative laser beams from a battery-powered hand-held laser prior to the topical application of OVA solution. The laser output consists of a total fifty-four 10 ms long pulsed beams, each with energy of 0.2 mJ, in a 6 × 9 array pattern over an area of 9 mm × 13 mm. The histological analysis showed no discernible damage in the epidermis and stratum corneum, which is consistent with previous studies.[22,32] Even with pretreatment of laser adjuvant,

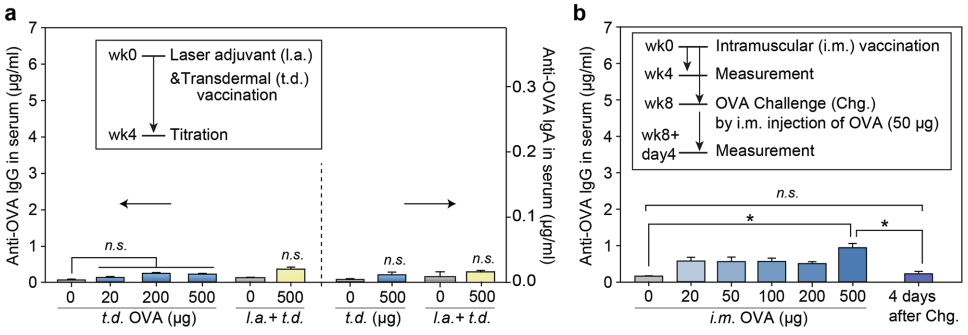

Figure 1. a) Induction of OVA-specific humoral and mucosal immune response four weeks after transdermal (t.d.) administration (blue), and laser-adjuvant (l.a.) transdermal administration (yellow) of OVA (mean ± SD, $n = 4$); n.s., $P > 0.05$. b) OVA-specific antibody titers measured at four weeks after intramuscular (i.m.) injection of OVA (500 μg) and 4 d after OVA challenge test (mean ± SD, $n = 4$); $^*P < 0.05$.

topical applications of OVA alone failed to induce a significant increase of antibody titers. This finding suggests that OVA alone cannot penetrate the skin barrier to induce immune response with or without laser adjuvants. It also indicates the intact skin barrier function after laser adjuvant.

Next, we tested intramuscular injection of native OVA alone. It has been reported that single intramuscular injection of OVA elicits limited antibody production, particularly without adjuvants.[33,34] In agreement with these results, we found that while IgG antibody production was higher than transdermal delivery at the same doses, the overall response was minimal and not significantly different from baseline at doses less than 500 μg (Figure 1b). The injection of a dose of 500 μg resulted in a moderately elevated IgG level at week 4, but failed to establish recall immunity against an OVA challenge (50 μg) test. This result indicates that the immunogenicity of OVA alone in the body is insufficient to stimulate efficient vaccination.

2.2. Synthesis of HA–OVA Conjugates

We synthesized HA–OVA conjugates using site-specific coupling reaction (Figure S1, Supporting Information; **Figure 2**a). Aldehyde (ALD) groups were introduced to HA molecules

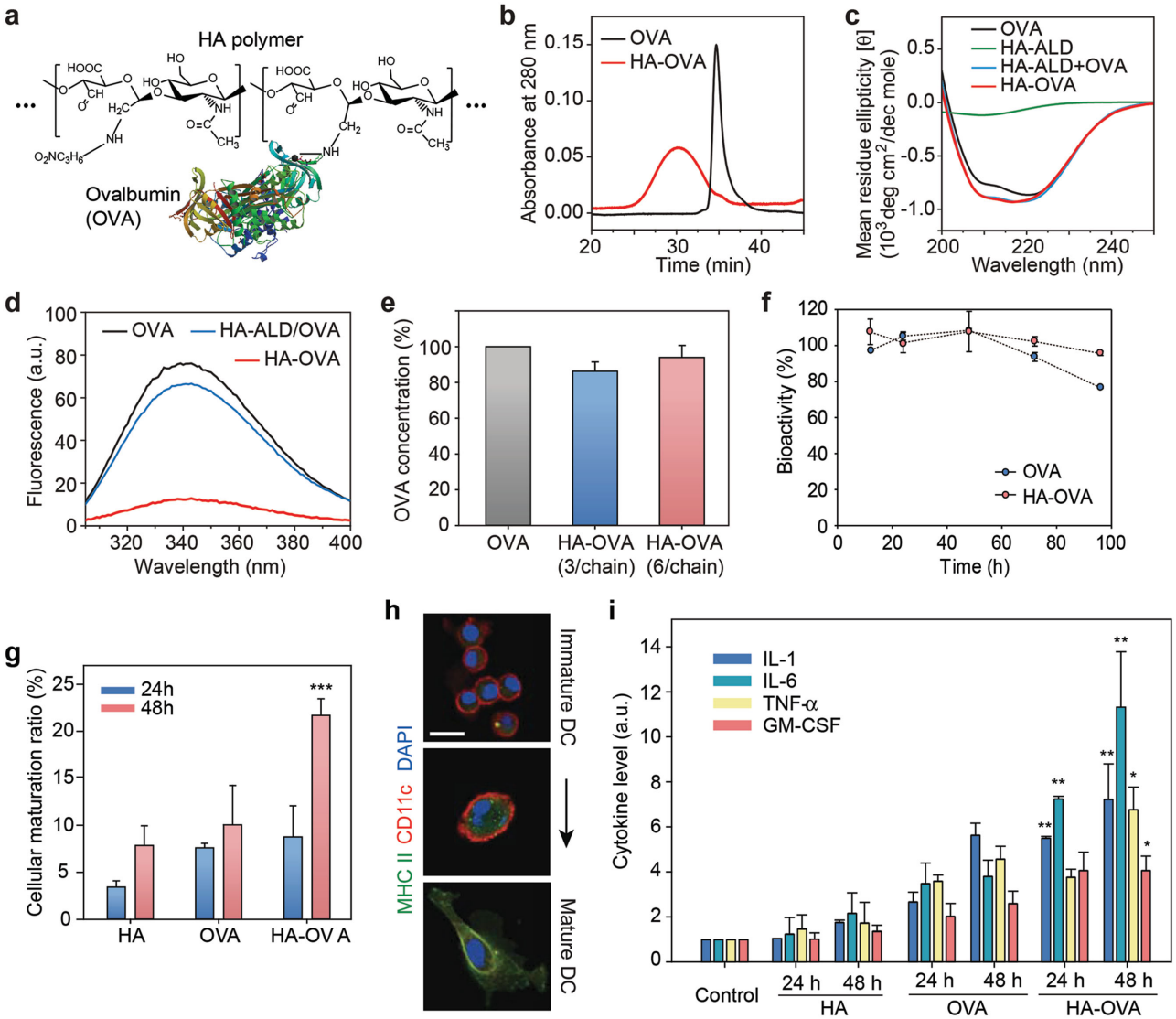

Figure 2. Characterization of HA–OVA conjugates. a) The chemical structure of HA–OVA conjugates. b) Gel permeation chromatograms of OVA (black) and HA–OVA conjugate (red). c) Circular dichroism spectra of OVA (black), HA–ALD (green), the mixture of OVA and HA–ALD (blue), and HA–OVA conjugates (red). d) Fluorescence emission spectra of OVA (black), the mixture of OVA and HA–ALD (blue), and HA–OVA conjugate (red). e) The ratio of bioactive OVA in HA–OVA. Error bars, s.d. f) In vitro stability of OVA and HA–OVA conjugates in human serum. g) The ratios of matured JAWS II cells 24 and 48 h after treatment with OVA, HA, and HA–OVA conjugates, respectively (mean ± SD, $n = 5$). $^{**}P < 0.01$, w.r.t. HA–OVA. h) Confocal fluorescence images of immature and matured DCs stained with anti-MHCII-Alexa 488 (green), anti-CD11c-Alexa 647 (red), and nuclear-dye Hoechst (blue). i) Cytokine levels measured by ELISA from JAWS II cells treated with OVA, HA, and HA–OVA conjugates for 24 h and 48 h (mean ± SD, $n = 5$). $^{*}P < 0.05$; $^{**}P < 0.01$, HA–OVA versus other groups. Scale bars: 10 μm in (h).

(215 kDa) by treatment with sodium periodate. The resulting HA–ALD was conjugated to the N-terminal primary amines of OVA at a low pH around 5 by using the pK_a difference between N-terminal primary amines and amines of lysine in OVA.[35] The retention time of HA–OVA conjugate in gel permeation chromatography (GPC) decreased after conjugation (Figure 2b), whereas the GPC peak unchanged for a simple mixture of OVA and HA–ALD (data are not shown). From the peak area of unreacted OVA before purification, the conjugation efficiency was calculated to be about 80%. The number of OVA per HA chain ranged from 3 to 6. The circular dichroism (CD) spectrum of OVA has a mixed secondary structure of α-helix and β-sheet,[36] and HA has a strong negative band at 210 nm.[37] The CD spectrum of HA–OVA conjugates matched well with that of the mixture of HA–ALD and unconjugated OVA (Figure 2c), which indicates that the secondary structure of OVA was maintained after conjugation. The peak of the fluorescence emission spectra of OVA and HA–OVA appeared at 355 nm, which corresponds to tryptophan (Trp) residues, indicating that the polarity of the microenvironment of Trp residues was not changed after conjugation (Figure 2d). The reduced fluorescence intensity of HA–OVA conjugates was likely due to quenching by interaction of OVA tryptophan residues with HA. Quenching of intrinsic protein fluorescence ascribed to interaction with several kinds of polymers has been reported elsewhere.[34] The immunological bioactivity of HA–OVA conjugates characterized by anti-OVA antibody in ELISA and Bradford assay was comparable to native OVA without conjugation (Figure 2e). HA–OVA conjugates exhibited excellent serum stability over 100 h, better than OVA (Figure 2f).

2.3. Cellular Uptake of HA–OVA In Vitro

To investigate cellular interaction of HA-OVA conjugates, we quantified the uptake of rhodamine B (RhoB) labeled OVA, HA, and HA–OVA conjugates by murine JAWS II dendritic cell line and human epidermal keratinocytes in vitro. Keratinocytes express HA receptors and contribute to antigen recognition by secreting immune mediators and transferring antigens to local DCs.[10,38] HA–OVA–RhoB and HA–RhoB conjugates entered these HA receptor-expressing cells much more efficiently than OVA–RhoB (Figure S2a, Supporting Information). When HA receptors, such as CD44, were blocked by pre-incubation of DCs and keratinocytes with an excessive amount of free HA, the cellular uptake of HA–OVA–RhoB conjugate was significantly reduced (Figure S2b, Supporting Information), which suggests that the endocytosis of HA–OVA conjugates is primarily mediated by HA receptors on the cell surface.[39] As the DCs matured, the number of major histocompatibility complex (MHC) Class II molecules on the cell surface increased.[40] HA–OVA conjugates induced 2.5-fold more maturation than OVA or HA alone 2 d after treatment (Figure 2g). The higher maturation efficiency suggests a role of HA in HA–OVA via HA receptor-mediated endocytosis. To characterize the response of immature DCs upon the uptake of HA–OVA conjugates, we imaged JAWS II cells for 2 d in vitro. Upon activation, the concentration of MHC class II in the cytoplasm increased considerably in the activated state (Figure 2h). We also measured

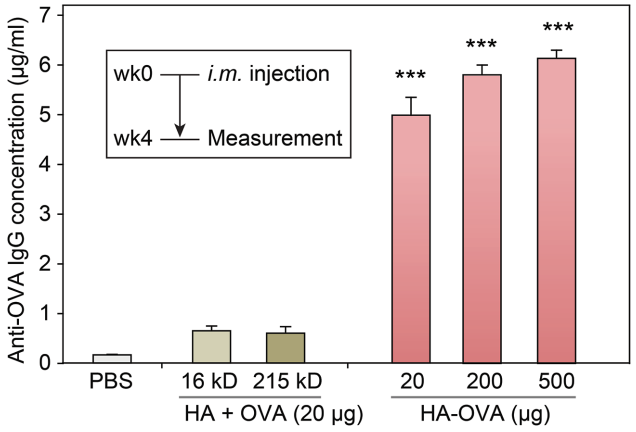

Figure 3. OVA-specific IgG antibody titers measured by ELISA four weeks after intramuscular (i.m.) injection of different agents (mean ± SD, $n = 4$). ***$P < 0.001$.

the levels of various pleiotropic cytokines, such as IL-1, IL-6, TNF-α, and granulocyte-macrophage colony-stimulating factor (GM–CSF), which are associated with the elevated expression of MHC class II molecules. HA–OVA conjugates significantly enhanced cytokine release from maturated DCs, more than HA or OVA alone (Figure 2i).

2.4. Intramuscular Immunization with HA–OVA In Vivo

We compared the effectiveness of HA–OVA with a mixture of OVA and HA in conventional intramuscular humoral immunization in mice (BALB/c). We found that anti-OVA IgG antibody titer in serum increased by 20-fold at four weeks after intramuscular injection of HA–OVA conjugate containing 20 μg of OVA, compared to normal levels in sham treated (PBS injected) animals (**Figure 3**). At higher doses of HA–OVA (200 or 500 μg of OVA), the serum IgG concentration only marginally increased further, indicating saturation of the antibody production. A simple mixture of OVA and free HA (16 or 215 kDa) failed to elicit IgG production. Similarly, in another study, trimethyl chitosan (TMC)–OVA conjugates have been shown to induce higher immune responses than the mixture of TMC and OVA.[34] These results confirm the synergistic adjuvant-like effect of HA in enhancing immunization efficiency.[34,41]

2.5. Transdermal Penetration of HA–OVA in Murine Skins In Vivo

To investigate the efficiency and dynamics of transdermal penetration, we topically applied RhoB conjugated OVA, HA, and HA–OVA, respectively, to mice (C57BL/6) at the back skin after carefully removing the hair by using an animal clipper.[42] Intravital two-photon microscopy showed time-dependent increase of HA–OVA–RhoB conjugate (red) in the dermis (**Figure 4**a). By contrast, the vast majority of OVA–RhoB did not penetrate the skin and remained in the stratum corneum (Figure 4b). Depth-resolved quantification of RhoB fluorescence intensity showed efficient penetration of HA–OVA–RhoB conjugate in

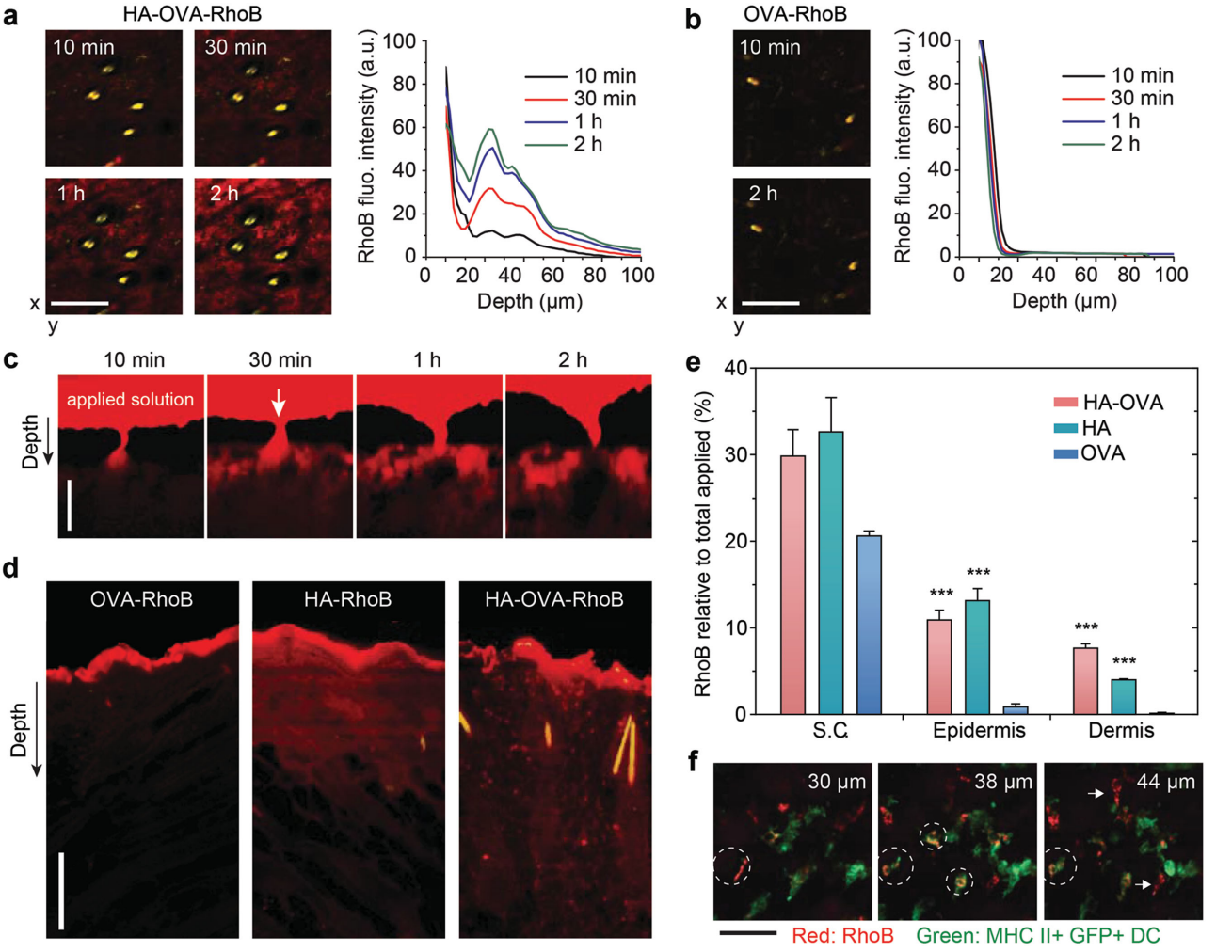

Figure 4. Two-photon excited fluorescence en face images and depth profiles of the murine skin in the dermis in vivo post-topical administration of a) HA–OVA–RhoB and b) OVA–RhoB conjugates. c) In vivo time-lapse images of HA–OVA–RhoB conjugate after topical administration. On top of the tissue, a reservoir of the applied agent in solution (red) is seen. Arrow indicates the position of a wrinkle line. d) Confocal fluorescence images of histological sections harvested 4 h after the topical application of OVA–RhoB, HA–RhoB, and HA–OVA–RhoB conjugates, respectively. e) Quantification of RhoB fluorescence intensity in the stratum corneum (S.C.), epidermis, and dermis layers. One hundred percent represents the total amount applied to the skin including that remaining in solution (see the text) (mean ± SD, $n = 7$). ***P-value < 0.001 w.r.t. OVA–RhoB. f) Z-sectioned confocal images of HA–OVA–RhoB conjugate (red) and MHC class II$^+$ eGFP$^+$ DCs (green) in the dermis in vivo. White dashed circles mark dermal DCs associated with HA–OVA–RhoB conjugate, and white arrows indicate the interaction of HA–OVA–RhoB conjugate presumably with other HA-receptor expressing cells, such as fibroblasts. Scale bars: a,b) 100 μm; c,d) 25 μm; f) and 50 μm.

stark contrast to the limited penetration of OVA–RhoB. The depth profile exhibited noticeable spatial heterogeneity, indicating there might be preferred routes for transdermal delivery. Examining hair follicles in the skin, we did not observe any apparent sign of penetration of HA–OVA–RhoB conjugate through the skin layer surrounding the hair follicles, contrary to the previous hypothesis of interfollicular delivery.[43] Unexpectedly, time-lapse images suggested that the initial primary delivery route is associated with natural wrinkles. The penetrated HA–OVA–RhoB conjugates through wrinkles diffuse rapidly throughout the dermis (Figure 4c). Interestingly, HA–OVA–RhoB conjugate was hardly detected in the epidermis within 2 h after topical application (Figure 4c).

Confocal images of tissue sections harvested at 4 h after topical administration showed significant penetration of HA–OVA–RhoB and HA–RhoB conjugates into both epidermis and dermis, whereas OVA–RhoB remained largely in the stratum corneum (Figure 4d). The images showed that, following the initial penetration through the wrinkles, HA–OVA conjugates (50 μg OVA) diffused directly from the stratum corneum to epidermis after a few hours of topical administration. At 4 h, the remaining solution outside the skin was collected, and we measured that 78% of the total applied OVA, 50% of HA, and 51% of HA–OVA, respectively, remained in the solution. Assuming that the rest of agents had penetrated in the tissues and analyzing the spatial distribution of RhoB fluorescence, we determined that 21% of the total OVA–RhoB was present in the stratum corneum, 0.9% in the epidermis, and 0.1% in the dermis (Figure 4e). On the other hand, 33%, 13%, and 4% of HA–RhoB, and 30%, 11%, and 8% of HA–OVA–RhoB

conjugate were distributed in the stratum corneum, epidermis, and dermis, respectively (Figure 4e). Of the total 49% HA–OVA conjugates that were absorbed in the skin, about 39% (=19/49) of them were delivered to the epidermis and dermis in 4 h.

To visualize the interaction of HA–OVA conjugates with DCs in vivo, we imaged MHC class II enhanced green fluorescence protein transgenic mice 2–4 h after topical administration. Depth-resolved two-photon microscopy images showed the accumulation of HA–OVA–RhoB conjugates at the surface and in the cytoplasm of dermal DCs (Figure 4f). The result suggests that the maturation and activation of DCs upon interaction with HA–OVA conjugates occur in vivo.

2.6. Migration of Activated DCs to Draining Lymph nodes

Following antigen recognition in the skin, the activated DCs migrate from the antigen entry site to a draining lymph node (LN) where the antigens are presented to the naive T cells in the LN to initiate adaptive immune responses.[44] To confirm this essential step in immunization, cervical LNs, which are draining LNs of the back skin, were harvested at 2 d after topical administration. Fluorescence images of tissue sections of the LNs showed a large number of HA–OVA–RhoB conjugates, but almost no OVA–RhoB and HA–RhoB conjugates were detected in the LNs (**Figure 5**a). Considering the significant penetration (17%) of HA beyond the stratum corneum, the absence of HA in the LNs suggests that the transportation of HA–OVA conjugate to the LNs is predominantly cell-mediated rather than passive diffusion. To corroborate our imaging analyses, we treated fluorescein isothiocyanate (FITC) labeled HA–OVA conjugates (HA–OVA–FITC) at the abdominal flank skin and performed flow cytometry of the cells in the draining inguinal and nondraining cervical LNs collected at 2, 4, and 6 d (Figure 5b). The number of $CD11c^+$, MHC class II^+ DCs that are associated with HA–OVA–FITC conjugate (high FITC fluorescence), was as much as 7% (±3%) at day 2 in the draining LNs, much higher than ≈2% in the nondraining LNs, which decreased over time at days 4 and 6 (Figure 5c). We further investigated whether migratory DCs carrying HA–OVA–FITC conjugate was indeed originated in skin. The majority of FITC-high DCs was devoid of CD8 commonly expressed in LN-resident DCs (Figure 5d). No apparent correlation was found between CD103 (aE integrin)+ DCs[45] and HA–OVA–FITC conjugate. Taken together, the histology and cytometry data support that skin-resident DCs uptake HA–OVA conjugates, much more efficiently than free OVA or HA, and subsequently migrated to draining LNs.

2.7. Transdermal Immunization without Laser Adjuvants

We tested the effectiveness of transdermal immunization in mice (BALB/c). HA–OVA conjugates with different amounts

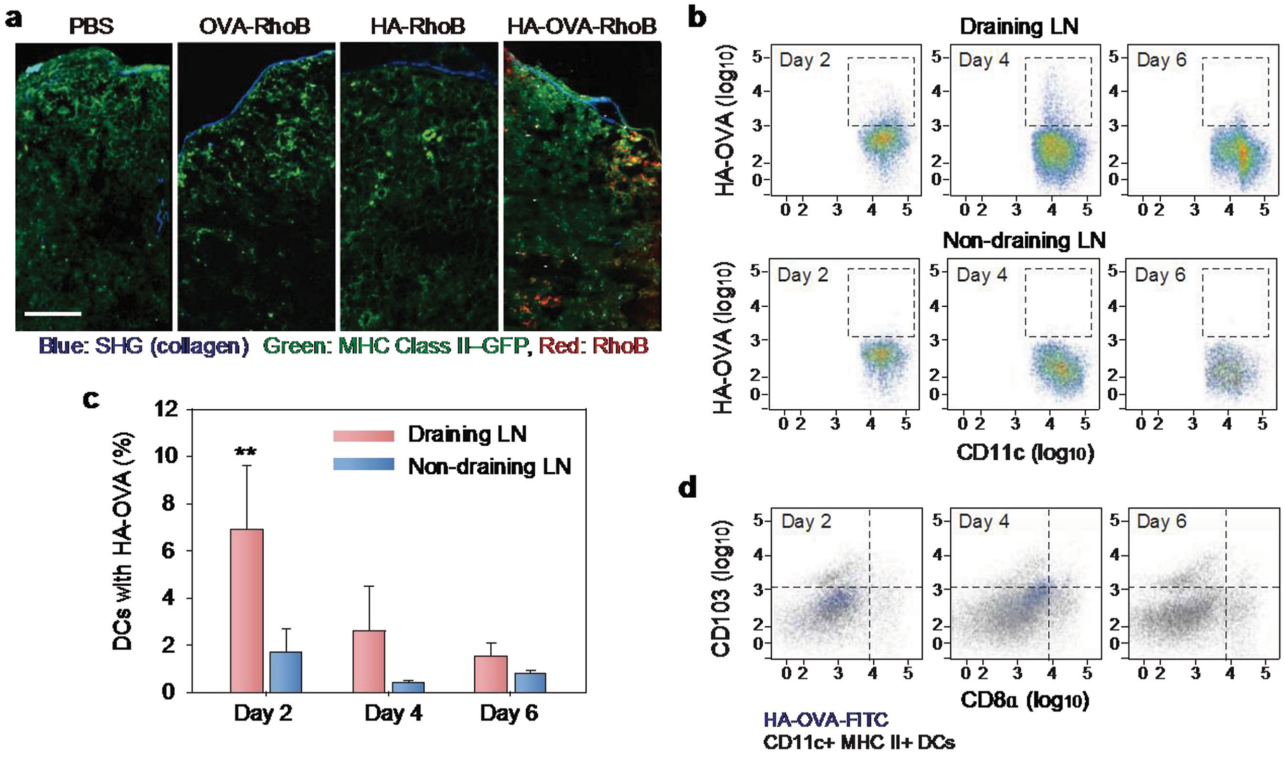

Figure 5. a) Two-photon microscopic image of histological sections of skin-draining LNs 2 d after treatment with PBS, OVA–RhoB, HA–RhoB, and HA–OVA–RhoB conjugates, respectively, on the back skin of mice. Scale bar: 100 μm. b) Cytometry plots of HA–OVA–FITC conjugate containing $CD11c^+$ DCs in skin draining LNs (top) and nondraining LNs (bottom), at 2, 4, and 6 d post-topical application on abdominal flank. c) The ratio of $CD11^+$ DCs containing HA–OVA–FITC conjugate determined from the cytometry results (mean ± SD, $n = 5$). $^{**}P < 0.01$, Draining LN versus Nondraining LN. d) Cytometry analysis for the expression of CD8α and CD103 of the cells associated with HA–OVA–FITC conjugate or $CD11c^+$ MHC II+, at 2, 4, and 6 d in draining LNs.

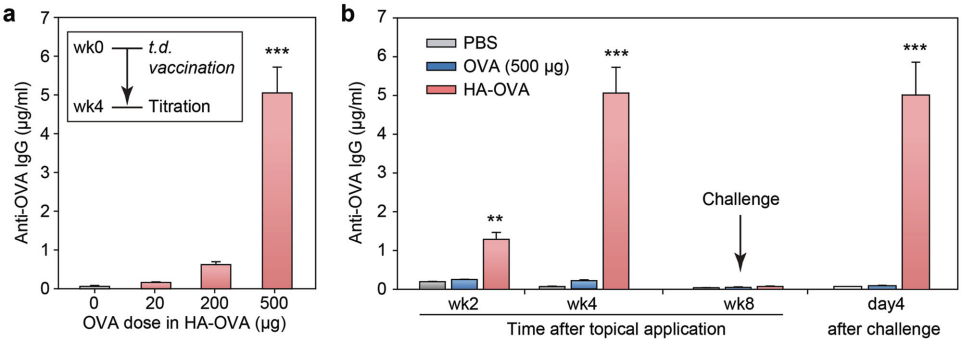

Figure 6. a) Induction of OVA-specific humoral immune response four weeks after transdermal (t.d.) administration of HA–OVA (mean ± SD, n = 4). ***P < 0.001, HA–OVA (500 μg of OVA) versus HA–OVA with other OVA doses. b) OVA-specific antibody titers measured at two, four, and eight weeks after transdermal immunization with HA–OVA conjugate (500 μg of OVA) (mean ± SD, n = 4) and 4 d after OVA challenge test. **P < 0.01; ***P < 0.001, HA–OVA versus OVA.

(20, 200, and 500 μg) of OVA were applied to the back skin of mice (n = 4 each). HA–OVA conjugates containing 20 μg of OVA showed minimal humoral responses. However, at higher doses of HA–OVA conjugate, significant anti-OVA IgG antibody titers were measured (**Figure 6**a).

Time-lapse titration measurement showed that the amount of anti-OVA IgG in the HA–OVA conjugate treated group peaked about four weeks after transdermal administration and decreased to a much lower nonimmunized (baseline) level at week 8 (Figure 6b). Having confirmed this duration, we tested immunologic memory in the mice that were vaccinated with various methods (n = 4 each), including transdermal administration of OVA and HA–OVA conjugate (500 μg of OVA). Eight weeks after vaccination, when the first immune response had disappeared, 50 μg of OVA was intramuscularly injected to each mouse, and the blood concentration of OVA specific antibody was measured 4 d after the immune challenge. Mice vaccinated by transdermal administration of HA–OVA conjugate with 500 μg of OVA showed a strong recall immune response, whereas all the other groups did not show significant antibody production (Figure 6b). The second immune response in the vaccinated group was considerably stronger than the first immune response, particularly in the early stages since the anti-OVA antibody concentration at 4 d postchallenge was as high as the maximum level achieved four weeks after initial topical administration (Figure 6b).

2.8. Transdermal Immunization by HA–OVA with Laser Adjuvants

The minimum OVA dose in HA–OVA required to induce strong immune responses via the intact skin was 500 μg (25 mg kg^{-1}), 25 times more than the dose of 20 μg (1 mg kg^{-1}) for intramuscular needle-based immunization (Figure 3). Considering the significant delivery efficiency of HA–OVA across the skin barrier (19% after 4 h in the epidermis and dermis; Figure 4f), we hypothesized that the large difference in the dose was in part due to the absence of needle-induced adjuvant effects in topical administration. HA–OVA solution was topically applied on back skin of BALB/c mice shortly after the illumination of laser adjuvant pulses (32 J total). Anti-OVA IgG titration in the serum obtained at four weeks after the immunization was significantly elevated from the control physiological level with an OVA dose of 20 μg (**Figure 7**). The IgG concentration at a dose of 50 μg was similar to those obtained with an intramuscular injection dose of 20 μg and transdermal dose of 500 μg without laser adjuvants. Anti-OVA IgA levels also showed a significant increase at a dose of 20 μg and further increased with the administered OVA amount in HA–OVA (Figure 7). Intramuscular immunization did not increase the IgA level, which is indicative of mucosal immunity.

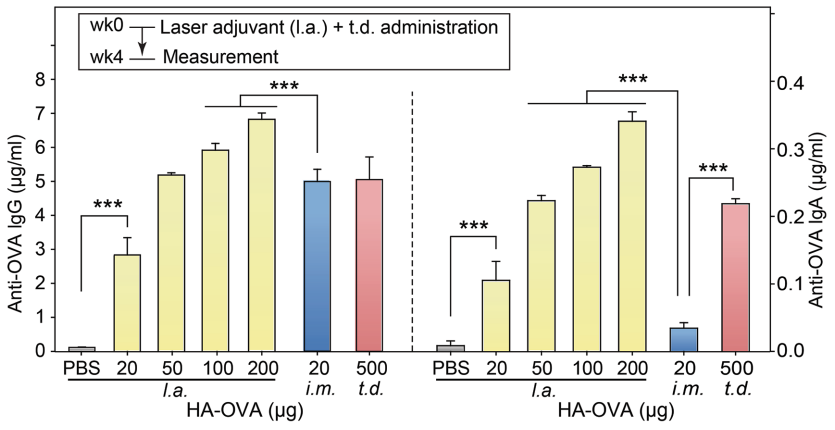

Figure 7. Concentration of OVA-specific IgG (left pannel) and IgA (right pannel) at four weeks after laser adjuvant (l.a.) and topical application of HA–OVA conjugates with various doses (mean ± SD, n = 4), in comparison to intramuscular (i.m.) injection and transdermal (t.d.) application without laser adjuvants. ***P < 0.001.

2.9. Transdermal Penetration of HA–OVA in Thick Porcine Skins

We also investigated the penetration efficiency of HA–OVA conjugates in porcine neck skins, which have a similar thickness and hair density to the human skin.[15]

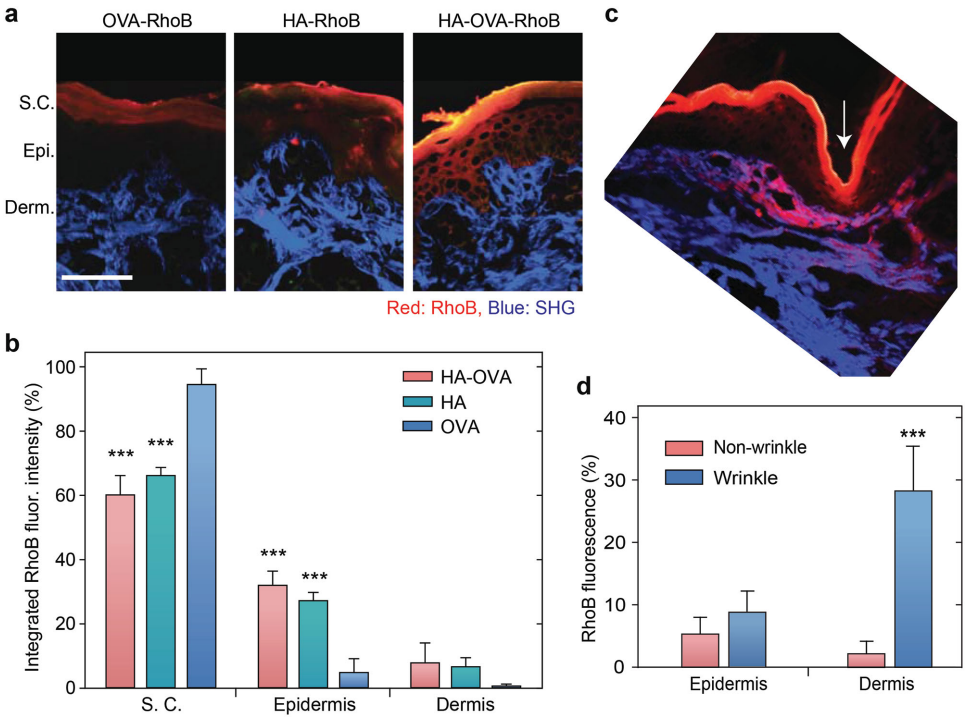

Figure 8. a) Two-photon microscope images of histological sections of porcine skins, 6 h after topical application of OVA–RhoB, HA–RhoB, and HA-OVA-RhoB conjugates, respectively. Red, RhoB fluorescence; blue, SHG from collagen fibers. S.C., stratum corneum; E., epidermis; D., dermis. Scale bar: 250 μm. b) Quantification of RhoB fluorescence intensity ratio integrated over stratum corneum, epidermis, and dermis, respectively, in the porcine skins (mean ± SD, $n = 7$). ***$P < 0.001$, w.r.t. OVA–RhoB. c) Two-photon image of histological section of porcine skin around wrinkle (white arrow) 2 h after topical application of HA–OVA–RhoB conjugate. d) Integrated RhoB fluorescence intensity over epidermis and dermis near wrinkles (white arrow in (c)) versus nonwrinkle regions (mean ± SD, $n = 7$). ***$P < 0.001$.

Two-photon microscopy images of the tissue sections obtained 6 h after a topical administration showed a marked penetration of HA–OVA conjugates into the epidermis and dermis (**Figure 8**a). Quantitative fluorescence analysis after anatomy-based image segmentation indicated that 60% of HA–OVA–RhoB was in the stratum corneum, 32% in epidermis, and 8% in dermis, whereas 95% of OVA–RhoB was confined in the stratum corneum (Figure 8b). Consistent with murine skins, we found indications of initial penetration of HA–OVA through wrinkles (Figure 8c). The enhanced penetration is attributed to the thinner epidermis around the wrinkles, which leads to short diffusion time across and high local concentration of HA–OVA conjugates in wrinkles; however, the possibility of higher permeability of the epithelia cell junction near wrinkles should not be ruled out.[46] HA–OVA conjugates accumulated in the dermis around wrinkles at 2 h (Figure 8d), but are expected to distribute more uniformly throughout the skin over time.

3. Discussion

Our results demonstrate the feasibility of a noninvasive, laser-assisted HA-based transdermal vaccination platform (**Figure 9**). When topically applied to intact skin by using a simple patch, more than 19% of HA–OVA conjugates penetrate to the epidermis and dermis in 4 h, and considerably more is likely delivered in 48 h. Laser adjuvant reduced the minimum dose of OVA from 25 to 1 mg kg^{-1}. In terms of the dose efficiency, the noninvasive transdermal platform is comparable to intramuscular injection of HA–OVA (1 mg kg^{-1}). Importantly, the dose efficiency is higher than conventional intramuscular injection of OVA alone. Furthermore, the transdermal immunization induced both systemic (lgG) and mucosal (lgA) immune responses, whereas intramuscular injection does not elicit the mucosal immune response.[10]

In addition to the role as nanocarriers for vaccines, HA provides additional benefit through an adjuvant-like effect, by promoting the presentation of the antigen to Langerhans and dermal DCs.[47] Despite the poor in vivo immunogenicity of OVA alone, conjugation of HA significantly enhanced vaccination efficiency. For intramuscular immunization, in which tissue penetration is not a factor, HA–OVA induced significantly higher immune response than OVA only and a simple mixture of OVA and HA. This result can be explained by the well-known role of HA as DAMP. Intrinsic HAs present in the healthy skin are polymers with high molecular weight (>1 MDa). At sites of inflammation, HA polymers are cleaved to smaller fragments, which are potent activators of DCs.[48] The HA repeating unit of *N*-acetyl-D-glucosamine can promote the maturation and activation of DCs in skin and stimulate T cells.[30,47] In addition, it has been shown that DCs are activated by HA via Toll-like receptor 4.[44]

While the present work has been focused on testing the proof-of-concept, the remarkable efficiency motivates in-depth studies of physiological and immunological responses and safety of the approach. Furthermore, it would warrant investigations for

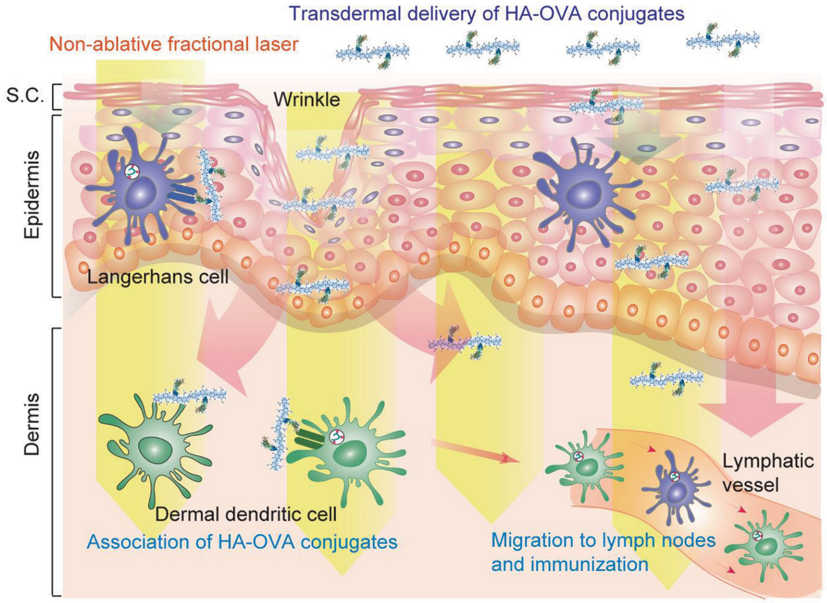

Figure 9. Schematic representation of transdermal immunization by HA–OVA conjugates with laser adjuvant. Topically applied HA–OVA conjugates penetrate into the skin through skin barriers and diffuse throughout the skin. Nonablative fractional laser adjuvant enhances immune response at the dermis layer. Activated dendritic cells (DCs) migrate to draining lymph nodes and induce immunity.

testing the practical potential of HA-conjugated vaccine patches. We found that HA-OVA conjugates were stable after freeze-drying at −20 °C. Various HA-conjugated vaccines may be distributed and stored in lyophilized powder forms, which can be readily dissolved in aqueous phase. The product can be easily sterilized using filter sterilization method same as other peptide or protein drugs.[49] The synthesis process does not require any specific reactors or complex purification steps, so scale-up manufacture can be easily set up. The dissolved HA vaccine can be easily applied to the skin in the forms of skin toners and lotions. In addition, HA vaccine conjugates can be prepared in a solution state for formulation due to the stable amide bond formation between HA and vaccine, which can be easily incorporated into skin vaccine patches.[9,50] Unlike conventional intramuscular and intranasal vaccination methods, non-invasive skin patches would not require highly trained personnel for administration and thus may enable simple administration at home. Studies have shown that about 93% of children experience serious immunization-related stress due to needle phobia,[51] and more than 10% of adults in the United States have needle fear.[52] Needle-free skin patches may encourage more people to take vaccination, ultimately reducing the healthcare costs. The combination of laser adjuvant and HA-vaccine patches may prove to be an attractive alternative to traditional intramuscular injection or emerging transdermal microneedle arrays.

4. Experimental Section

Synthesis and Labeling of HA–OVA Conjugates: Aldehyde-modified HA (HA–ALD) was synthesized as described elsewhere.[53] OVA (5 mg mL^{-1}) and HA–ALD with an aldehyde content of 15 mol% was dissolved in sodium acetate buffer (pH 5.0), and HA–OVA conjugate was formed by the coupling reaction between ALD of HA–ALD and the N-terminal amine group of OVA. After conjugation, 5 M excess of ethyl carbazate was added and stirred for 24 h to block the residual aldehyde group in HA–OVA conjugates. Sodium cyanoborohydride with 5 M excess of HA repeating unit was added for the reduction of hydrazine bonds at room temperature for 24 h. The resulting HA–OVA conjugate solution was filtered with a 0.45 μm syringe filter and purified using a centrifugal filter (MWCO of 50 kDa, Millipore, Darmstadt, Germany) to remove unreacted OVA and other chemicals. For bioimaging and FACS analysis, HA, OVA, and HA–OVA conjugate were labeled with Lissamine rhodamine B sulfonyl chloride (RhoB) or FITC. RhoB was dissolved in dimethylformamide at a concentration of 10 mg mL^{-1}, and 10 M excess of RhoB was added to the solutions of amine-modified HA, OVA, and HA–OVA conjugate dissolved in sodium carbonate buffer (pH 9.0), respectively. The reaction mixture stirred at room temperature for 2 h in the dark and purified using PD 10 desalting columns. The degree of labeling modification was assessed by measuring the absorbance at 280 and 540 nm. FITC was labelled using the same method as RhoB, but the degree of labeling modification was assessed by measuring the absorbance at 280 and 494 nm.

Characterization of HA–OVA Conjugates: The synthesized HA–OVA conjugates were characterized by GPC analysis by comparing the retention time before and after conjugation of HA and OVA. The bioconjugation efficiency of OVA was calculated by analyzing the GPC peak area of unreacted OVA before purification. GPC analysis was performed using the following systems: Waters 717 plus autosampler, Waters 1525 binary HPLC pump, Waters 2487 dual λ absorbance detector, and Ultrahydrogel 1000 connected with Ultrahydrogel 500 column. The mobile phase was PBS at pH 7.4 and the flow rate was 0.5 mL min^{-1}. The detection wavelength was 280 nm. The secondary structure of HA–OVA conjugate was analyzed by CD spectroscopy. CD spectra of HA–ALD, OVA, and HA–OVA conjugates, and the mixture of HA–ALD and OVA dissolved in PBS were obtained with a spectrum-polarimeter (J-715, JASCO, Easton, MD) at a step size of 0.5 nm. The microenvironment around Trp residues in OVA, HA–OVA conjugate, and the mixture of HA–ALD and OVA dissolved in PBS was assessed by fluorescence spectroscopy using a spectrofluorometer (Cary Eclipse Fluorescence Spectrophotometer, Agilent Technologies, Santa Clara, CA) with excitation at 280 nm. The immunological affinity of OVA and HA–OVA conjugates to anti-OVA antibody was assessed by OVA ELISA based on the absorbance at 450 nm with a microplate reader (SpectraFluor Plus, TECAN, Mannedorf, Switzerland). The serum stability of OVA and HA–OVA was evaluated by ELISA after incubation in human serum at a concentration of 0.5 mg mL^{-1} and 37 °C for up to 4 d.

In Vitro Immunization of HA–OVA Conjugates: To assess the maturation of DCs, treated JAWS II cells were stained with MHC-class-II antibody-Alexa 488, CD11c antibody-Alexa 647 conjugates, and DAPI for 1 h, and washed with PBS. Cell morphologies were observed with a confocal microscope (FV1000, Olympus America Inc., Tokyo, Japan). The matured DCs were counted from microscope images. In addition, in vitro immunization was assessed by measuring the amount of cytokine and chemokine from 10^5 JAWS II cells. HA, OVA, and HA–OVA conjugates in 500 μL of α-MEM containing 2 vol% Fetal Bovine Serum (FBS) with ribonucleosides, deoxyribonucleosides, 4×10^{-3} M L-glutamine, 1×10^{-3} M sodium pyruvate, and 5 ng mL^{-1} murine GM-CSF were added to the cells in culture plates and incubated for 12 h, followed by the addition of 500 μL culture medium. At 1 and 2 d after treatment, respectively, samples of the incubation medium (100 μL) were collected and the

whole medium was replaced with 100 µL of fresh 2% FBS containing medium. The amount of cytokine and chemokine in the samples was measured by using ELISA.

Mice: Eight-week-old wild-type BALB/c mice for investigating immune response, wild-type C57BL/6 mice for investigating skin penetration through imaging, and MHC class II$^+$ eGFP$^+$ transgenic mice in C57BL/6 background[54] bred in pathogen-free facilities at Harvard Medical School (HMS) and Pohang University of Science and Technology (POSTECH) were used in this study. All live animal experiments were approved by the HMS Institutional Animal Care and Use Committee (#05052) and the Ethics Committee of POSTECH.

Fluorescence Imaging of Transdermal Delivery: PBS, OVA–RhoB, HA–RhoB, or HA–OVA–RhoB conjugates containing the same amount of OVA (50 µg) and HA (100 µg) was topically applied on the hair-removed mouse skin. An adhesive patch was attached onto the applied area to minimize drying. The retrieved skin tissues after 4 h were fixed in 4% paraformaldehyde solution, embedded into optimal cutting temperature (OCT) compound at −70 °C, and cut into 5 µm thick sections. The sections were fixed with cold acetone at −20 °C and washed with distilled water to remove the residual OCT resins on the slide. Histological tissue sections were imaged by using a home-built confocal microscope. For intravital microscopy, the hair in the dried skin on the back was removed carefully using an electrical animal clipper, which maintains the barrier function of the stratum corneum. Depilating agents were not used to exclude any potential effects on DCs in the skin.[55] Anesthetized MHC class II$^+$ eGFP$^+$ mice were placed on a temperature-controlled stage. OVA–RhoB or HA–OVA–RhoB conjugates were applied to the shaved and intact skin. In vivo imaging was performed with a custom-built, video-rate, two-photon microscope using a Ti:Sapphire laser (Mai-Tai DeepSee, Spectra-Physics, Santa Clara, CA) and a water immersion objective lens (20×, 0.9 NA), as previously described.[56] The excitation wavelength was set to 810 nm, and the optical power at the sample was ≈150 mW. The image analysis and the generation of time-lapse image sequences were performed using Image J and custom software.

LN Analysis: Histological analysis of dissected cervical LNs was carried out with a home-built two-photon microscope 2 d post-topical administration at the back neck skin of MHC class II$^+$ eGFP$^+$ mice. For further flow cytometric analysis, 0.5 mg of FITC-conjugated HA–OVA conjugates were applied to the abdonimal flank skin, and draining inguinal LNs were collected 2, 4, and 6 d. The cells from the tissues were stained with allophycocyanin-conjugated anti-CD11c, pacific blue-conjugated anti-IA/IE, phycoerythrin-cyanin7-conjugated anti-CD8α, and phycoerythirin-conjugated anti-CD103 (all from eBioscience, San Diego, CA), and analyzed by flow cytometry using BD FACSCanto II (BD Bioscience, San Diego, CA) and FlowJo program (FlowJo, LLC, Ashland, OR).

Laser Adjuvant: A commercial battery-powered hand-held laser device (PaloVia Skin Renewing System, Palomar medical technologies), which has been originally approved and marketed for home skin care,[57] was used for laser adjuvant. Upon each trigger, the device emits a 6 × 9 array of laser beams at a center wavelength 1410 nm (± 20 nm) for a pulse duration of 10 ms. The pulse energy was set to 0.2 mJ per pulse. The pulse energy, duration, wavelength, and beam focal depth were optimized so that the nonablative beam affects the dermis while leaving the skin surface intact. After the laser head was made in contact to the hair-shaved skin, the device was triggered three times depositing about 32.4 mJ of optical energy to a 9 mm by 13 mm area. Its adjuvant effects on APCs is described in detail elsewhere.[21,22]

In Vivo Immunization and Sample Collection: In vivo immunization experiments were carried out using BALB/c mice with a mean body weight of 20 g. HA–OVA conjugates (20 µg of OVA) were administered using a needle intramuscularly. Topical transdermal administration was conducted with HA–OVA conjugate containing 20, 200, or 500 µg of OVA. The skin patch covering the applied agents was removed after 48 h. For comparison, free OVA at various doses (20, 200, and 500 µg) were administered using the same protocol. Laser-adjuvant was given to the skin before the topical treatment of HA–OVA conjugates. Blood samples were harvested four weeks postadministration of OVA and HA–OVA conjugates. In addition, to investigate time dependence of immune responses, blood samples were collected two, four, and eight weeks after administration, respectively. In addition, to estimate mucosal immunity, BAL fluid also collected as described elsewhere.[15,58] To investigate recall immune response, 50 µg of OVA was injected into the mice eight weeks after topical application of OVA and HA–OVA conjugates (500 µg of OVA). Four days after the immune challenge, blood samples were harvested and analyzed for humoral immune responses.

Anti-OVA IgG and IgA Analysis: The immunization of HA–OVA conjugates was evaluated by anti-OVA IgG and IgA antibody ELISA. OVA solution at a concentration of 10 µg mL^{-1} in sodium carbonate buffer was incubated in 96-well plate for 1 h at room temperature. After washing thrice with Tris-buffered saline and Tween 20 (TTBS), the wells were incubated with 1% skim milk. After washing with TTBS, anti-mouse OVA antibody standard solutions and blood samples diluted in PBS were added to the well and incubated at room temperature for 1 h. After washing with TTBS, goat anti-mouse IgG antibody-HRP conjugate solution at a concentration of 0.3 µg mL^{-1} in PBS was added to the well and incubated at room temperature for 1 h. Finally, after washing with TTBS, the wells were incubated with TMB solution followed by 2 N H_2SO_4 stop solution. The absorbance was measured at 450 nm with a microplate reader. ELISA was performed twice with four replicates. In case of IgA, we carried out same procedure using anti-mouse IgA antibody–HRP conjugates.

Porcine Experiment: Porcine neck skin tissues (10 × 10 cm^2 each) were extracted from three-month-old pigs immediately after postmortem at Knight Laboratory in the Department of Surgery at MGH, as approved by the MGH Subcommittee on Research Animal Care (#2014N000049). After hair-removal of the porcine skin using animal clipper,[42] OVA–RhoB or HA–OVA-RhoB (250 µg of OVA each) was topically applied to the 2 cm wide central regions of the tissues. At different time points (2–6 h) after administration, cross-sectional tissue sections were obtained and analyzed by two-photon microscopy.

Statistical Analysis: Data are expressed as means ± standard deviation from several animals in a group in a few separate experiments. Statistical analysis was carried out with the two-way analysis of variance test using SigmaPlot10.0 (Systat Software, Inc., San Jose, CA). *P* values less than 0.05 were considered statistically significant.

Supporting Information

Supporting Information is available from the Wiley Online Library or from the author.

Acknowledgements

K.S.K. and H.K. contributed equally to this work. The authors thank Dr. Myunghwan Choi and Dr. Jie Zhao for help in intravital imaging and histological analysis, Dr. Mark Randolph for providing access to experimental pigs, Dr. Jeesoo An for help in interpretation of histology, and Dr. Ji Wang and Prof. Mei Wu for discussion. This study was supported by Mid-career Researcher Program through the National Research Foundation of Korea grant funded by the Ministry of Education, Science and Technology (Grant No. 2012R1A2A2A06045773) and in part by National Institutes of Health (Grant Nos. P41-EB015903, R01-CA192878, P01-HL120839).

Received: November 13, 2015
Revised: December 17, 2015
Published online: February 1, 2016

[1] S. A. Plotkin, *Nat. Med.* **2005**, *11*, S5.
[2] a) J. J. Moon, H. Suh, A. Bershteyn, M. T. Stephan, H. Liu, B. Huang, M. Sohail, S. Luo, S. Ho Um, H. Khant, J. T. Goodwin,

J. Ramos, W. Chiu, D. J. Irvine, *Nat. Mater.* **2011**, *10*, 243; b) M. F. Bachmann, G. T. Jennings, *Nat. Rev. Immunol.* **2010**, *10*, 787.
[3] R. T. Kenney, S. A. Frech, L. R. Muenz, C. P. Villar, G. M. Glenn, *New Engl. J. Med.* **2004**, *351*, 2295.
[4] D. Chen, R. L. Endres, C. A. Erickson, K. F. Weis, M. W. McGregor, Y. Kawaoka, L. G. Payne, *Nat. Med.* **2000**, *6*, 1187.
[5] B. E. Polat, D. Hart, R. Langer, D. Blankschtein, *J. Controlled Release* **2011**, *152*, 330.
[6] L. A. Hirao, L. Wu, A. S. Khan, A. Satishchandran, R. Draghia-Akli, D. B. Weiner, *Vaccine* **2008**, *26*, 440.
[7] D. Pissuwan, K. Nose, R. Kurihara, K. Kaneko, Y. Tahara, N. Kamiya, M. Goto, Y. Katayama, T. Niidome, *Small* **2011**, *7*, 215.
[8] V. P. Torchilin, *Nat. Rev. Drug Discov.* **2005**, *4*, 145.
[9] X. Su, B.-S. Kim, S. R. Kim, P. T. Hammond, D. J. Irvine, *ACS Nano* **2009**, *3*, 3719.
[10] Y. Huang, Y. S. Park, C. Moon, A. E. David, H. S. Chung, V. C. Yang, *Angew. Chem. Int. Ed.* **2010**, *49*, 2724.
[11] R. Rappuoli, C. W. Mandl, S. Black, E. De Gregorio, *Nat. Rev. Immunol.* **2011**, *11*, 865.
[12] G. Rechtsteiner, T. Warger, P. Osterloh, H. Schild, M. P. Radsak, *J. Immunol.* **2005**, *174*, 2476.
[13] G. M. Glenn, D. N. Taylor, X. Li, S. Frankel, A. Montemarano, C. R. Alving, *Nat. Med.* **2000**, *6*, 1403.
[14] N. Petrovsky, J. C. Aguilar, *Immunol. Cell Biol.* **2004**, *82*, 488.
[15] S. P. Sullivan, D. G. Koutsonanos, M. Del Pilar Martin, J. W. Lee, V. Zarnitsyn, S. O. Choi, N. Murthy, R. W. Compans, I. Skountzou, M. R. Prausnitz, *Nat. Med.* **2010**, *16*, 915.
[16] a) P. C. DeMuth, Y. Min, B. Huang, J. A. Kramer, A. D. Miller, D. H. Barouch, P. T. Hammond, D. J. Irvine, *Nat. Mater.* **2013**, *12*, 367; b) V. Bachy, C. Hervouet, P. D. Becker, L. Chorro, L. M. Carlin, S. Herath, T. Papagatsias, J. B. Barbaroux, S. J. Oh, A. Benlahrech, T. Athanasopoulos, G. Dickson, S. Patterson, S. Y. Kwon, F. Geissmann, L. S. Klavinskis, *Proc. Natl. Acad. Sci. USA* **2013**, *110*, 3041.
[17] T. S. Kupper, R. C. Fuhlbrigge, *Nat. Rev. Immunol.* **2004**, *4*, 211.
[18] X. Chen, P. Kim, B. Farinelli, A. Doukas, S.-H. Yun, J. A. Gelfand, R. R. Anderson, M. X. Wu, *PLoS One* **2010**, *5*, e13776.
[19] X. Chen, D. Shah, G. Kositratna, D. Manstein, R. R. Anderson, M. X. Wu, *J. Controlled Release* **2012**, *159*, 43.
[20] S. Kashiwagi, J. Yuan, B. Forbes, M. L. Hibert, E. L. Q. Lee, L. Whicher, C. Goudie, Y. Yang, T. Chen, B. Edelblute, B. Collette, L. Edington, J. Trussler, J. Nezivar, P. Leblanc, R. Bronson, K. Tsukada, M. Suematsu, J. Dover, T. Brauns, J. Gelfand, M. C. Poznansky, *PloS One* **2013**, *8*, e82899.
[21] J. Wang, B. Li, M. X. Wu, *Proc. Natl. Acad. Sci. USA* **2015**, *112*, 5005.
[22] J. Wang, D. Shah, X. Chen, R. R. Anderson, M. X. Wu, *Nat. Commun.* **2014**, *5*, 4447.
[23] T. J. Brown, D. Alcorn, J. R. Fraser, *J. Invest. Dermatol.* **1999**, *113*, 740.
[24] M. B. Brown, S. A. Jones, *J. Eur. Acad. Dermatol. Venereol.* **2005**, *19*, 308.
[25] R. Tammi, A. M. Saamanen, H. I. Maibach, M. Tammi, *J. Invest. Dermatol.* **1991**, *97*, 126.
[26] M. Witting, A. Boreham, R. Brodwolf, K. Vavrova, U. Alexiev, W. Friess, S. Hedtrich, *Mol. Pharmaceutics* **2015**, *12*, 1391.
[27] J. A. Yang, E. S. Kim, J. H. Kwon, H. Kim, J. H. Shin, S. H. Yun, K. Y. Choi, S. K. Hahn, *Biomaterials* **2012**, *33*, 5947.
[28] M. Singh, M. Briones, D. T. O'Hagan, *J. Controlled Release* **2001**, *70*, 267.
[29] H. S. Jung, W. H. Kong, D. K. Sung, M.-Y. Lee, S. E. Beack, D. H. Keum, K. S. Kim, S. H. Yun, S. K. Hahn, *ACS Nano* **2014**, *8*, 260.
[30] C. Termeer, F. Benedix, J. Sleeman, C. Fieber, U. Voith, T. Ahrens, K. Miyake, M. Freudenberg, C. Galanos, J. C. Simon, *J. Exp. Med.* **2002**, *195*, 99.
[31] a) H. Kono, K. L. Rock, *Nat. Rev. Immunol.* **2008**, *8*, 279; b) D. Jiang, J. Liang, J. Fan, S. Yu, S. Chen, Y. Luo, G. D. Prestwich, M. M. Mascarenhas, H. G. Garg, D. A. Quinn, R. J. Homer, D. R. Goldstein, R. Bucala, P. J. Lee, R. Medzhitov, P. W. Noble, *Nat. Med.* **2005**, *11*, 1173.
[32] J. Leyden, T. J. Stephens, J. H. Herndon Jr., *J. Am. Acad. Dermatol.* **2012**, *67*, 975.
[33] D. M. Klinman, K. M. Barnhart, J. Conover, *Vaccine* **1999**, *17*, 19.
[34] B. Slutter, P. C. Soema, Z. Ding, R. Verheul, W. Hennink, W. Jiskoot, *J. Controlled Release* **2010**, *143*, 207.
[35] a) O. Kinstler, G. Molineux, M. Treuheit, D. Ladd, C. Gegg, *Adv. Drug Deliv. Rev.* **2002**, *54*, 477; b) L. Tao, G. Mantovani, F. Lecolley, D. M. Haddleton, *J. Am. Chem. Soc.* **2004**, *126*, 13220.
[36] E. Eiser, C. S. Miles, N. Geerts, P. Verschuren, C. E. MacPhee, *Soft Matter* **2009**, *5*, 2725.
[37] K. Burger, J. Illes, B. Gyurcsik, M. Gazdag, E. Forrai, I. Dekany, K. Mihalyfi, *Carbohydr. Res.* **2001**, *332*, 197.
[38] G. R. Leggatt, L. A. Dunn, R. L. De kluyver, T. Stewart, I. H. Frazer, *Immunol. Cell Biol.* **2002**, *80*, 415.
[39] Y. Do, P. S. Nagarkatti, M. P. Nagarkatti, *J. Immunother.* **2004**, *27*, 1.
[40] J. A. Villadangos, M. a. Cardoso, R. J. Steptoe, D. van Berkel, J. Pooley, F. R. Carbone, K. Shortman, *Immunity* **2001**, *14*, 739.
[41] F. Y. Avci, X. Li, M. Tsuji, D. L. Kasper, *Nat. Med.* **2011**, *17*, 1602.
[42] P. Karande, A. Jain, S. Mitragotri, *Nat. Biotech.* **2004**, *22*, 192.
[43] H. Fan, Q. Lin, G. R. Morrissey, P. A. Khavari, *Nat. Biotechnol.* **1999**, *17*, 870.
[44] S. Henri, L. F. Poulin, S. Tamoutounour, L. Ardouin, M. Guilliams, B. de Bovis, E. Devilard, C. Viret, H. Azukizawa, A. Kissenpfennig, B. Malissen, *J. Exp. Med.* **2010**, *207*, 189.
[45] S. Bedoui, P. G. Whitney, J. Waithman, L. Eidsmo, L. Wakim, I. Caminschi, R. S. Allan, M. Wojtasiak, K. Shortman, F. R. Carbone, A. G. Brooks, W. R. Heath, *Nat. Immunol.* **2009**, *10*, 488.
[46] Y. Wang, K. L. Marshall, Y. Baba, G. J. Gerling, E. A. Lumpkin, *PloS One* **2013**, *8*, e67439.
[47] J. Muto, Y. Morioka, K. Yamasaki, M. Kim, A. Garcia, A. F. Carlin, A. Varki, R. L. Gallo, *J. Clin. Invest.* **2014**, *124*, 1309.
[48] C. C. Termeer, J. Hennies, U. Voith, T. Ahrens, J. M. Weiss, P. Prehm, J. C. Simon, *J. Immunol.* **2000**, *165*, 1863.
[49] A. K. Banga, *Therapeutic Peptides and Proteins: Formulation, Processing, and Delivery Systems*, CRC Press, Boca Raton, FL, USA **2006**.
[50] Y. Ishii, T. Nakae, F. Sakamoto, K. Matsuo, K. Matsuo, Y.-S. Quan, F. Kamiyama, T. Fujita, A. Yamamoto, S. Nakagawa, N. Okada, *J. Controlled Release* **2008**, *131*, 113.
[51] a) M. Ives, S. Melrose, *Nurs. Forum* **2010**, *45*, 29; b) S. C. Kettwich, W. L. Sibbitt, J. R. Brandt, C. R. Johnson, C. S. Wong, A. D. Bankhurst, *J. Pediatr. Oncol. Nurs.* **2007**, *24*, 20.
[52] J. G. Hamilton, *J. Fam. Practice* **1995**, *41*, 169.
[53] J. A. Yang, K. Park, H. Jung, H. Kim, S. W. Hong, S. K. Yoon, S. K. Hahn, *Biomaterials* **2011**, *32*, 8722.
[54] M. Boes, J. Cerny, R. Massol, M. Op den Brouw, T. Kirchhausen, J. Chen, H. L. Ploegh, *Nature* **2002**, *418*, 983.
[55] D. Sen, L. Forrest, T. B. Kepler, I. Parker, M. D. Cahalan, *Proc. Natl. Acad. Sci. USA* **2010**, *107*, 8334.
[56] M. Choi, S. H. Yun, *Opt. Express* **2013**, *21*, 30842.
[57] D. Manstein, G. S. Herron, R. K. Sink, H. Tanner, R. R. Anderson, *Lasers Surg. Med.* **2004**, *34*, 426.
[58] J. Bessa, A. Jegerlehner, H. J. Hinton, P. Pumpens, P. Saudan, P. Schneider, M. F. Bachmann, *J. Immunol.* **2009**, *183*, 3788.